Numerical Studies of Performance Variations in the Combustion of 100% Biojet Fuel in a Jet Engine

E. J. K. Nilsson & C. Fureby

Project: **Numerical studies of performance variations in the combustion of 100% biojet fuel in a jet engine**
Project number: **52448-1**
Date: **2023-03-19**
Funding Source: **The Swedish Energy Agency**
Project coordinator: **Lund University, Dept. of Heat Transfer**

LUND UNIVERSITY

Faculty of Engineering, LTH
Division of Heat Transfer
Division of Combustion Physics
Box 118, 221 00 LUND, Sweden
https://www.ht.energy.lth.se/english/

Numerical Studies of Performance Variations in the Combustion of 100% Biojet Fuel in a Jet Engine

M. Passad[†], A. Åkerblom[‡], E. Nilsson[†] & C. Fureby[‡]
[‡]Lund University, Energy Sciences, Lund, PO Box 118, SE 221-00, Sweden
[†]Lund University, Combustion Physics, Lund, PO Box 118, SE 221-00, Sweden

1. Introduction

In recent years, aviation has explored alternatives to fossil jet fuel to reduce its environmental impact and to ensure security-of-supply at affordable prices. Sweden has set an ambitious target by enforcing the use of drop-in bio-jetfuels from January 2021, gradually increasing from 1% to 30% in 2030. Production of these sustainable or renewable bio-jetfuels is challenging in terms of feedstocks and production methods, and the resulting bio-jetfuel is different from the fossil jet fuel. To increase the understanding of combustion of renewable fuels in existing jet engines, numerical models can be used to analyze and optimize combustion and subsequently also emissions. The advantage of numerical studies is the possibility to test many fuels, also fuels that are not yet produced in large enough amounts for testing to be performed, which would be difficult or even impossible to study experimentally. Instead carefully designed experimental studies can be conducted on fuels that have been selected based on a modeling-based pre-screening.

The present work is a contribute to the development of 100% renewable fuels for aviation, by combustion studies using numerical simulation. Here, Large Eddy Simulation (LES) methods are employed to simulate three selected flame configurations, representative to aero engines and aero engine derivatives, providing both validation and insight into the combustion of bio-jetfuels. To take the fuel properties into account it is necessary to include chemical kinetics mechanisms and transport properties for each jet fuel. All numerical simulation studies performed in this work include the conventional fossil Jet A fuel as a reference, and also the fossil JP5 fuel that is more common in military applications. These conventional fossil fuels are compared to two types of bio jet fuels, hereafter denoted C1 and C5. But also single component fuels n-heptane and dodecane as representatives for components of the jet fuels, they are also useful for validation of modeling approaches since experimental data exist and the understanding of the combustion chemistry is good. For the mentioned fuels we map similarities and differences in combustion behavior compared to Jet A. This report contains an overview literature study about jet fuel properties, brief results from 0D and 1D studies of ignition and laminar flames, and LES-based numerical simulation studies of three jet engine combustion configurations.

2. Fossil and Sustainable Jet Fuels

We start by reviewing the different types of fossil and sustainable jet fuels present today and under research and development. This typically involves conventional petroleum-based jet fuels and alternative, sustainable, non-fossil based jet fuels from a variety of feedstocks being processed and blended into jet fuels using different process technologies.

2.1. Fossil Jet Fuels

Jet fuel is a multi-component fuel with a carbon chain length of C8-C16, [1], which has originally been developed from lamp oil. The specification of jet fuel has developed and changed in line with the jet engine evolution, safety and security of supply criteria, [2]. Jet fuels are kerosene-based fuels derived from petroleum. Most often, Jet A and Jet A1 are used in commercial flights, and JP8 is its military counterpart, containing additives for corrosion and static protections. The difference between Jet A and Jet A1 is that Jet A1 has lower freezing point, making it more suitable for intercontinental flights. JP5 is a similar jet fuel often used for navy applications due to it being more difficult to ignite, making it more suited for navy use.

Between 70% and 85% of the jet fuel is made up of normal, and iso-paraffins, with cyclo-paraffins and aromatics also being present. The division between n- and iso-paraffins is variable and depends on the crude supplied to the refinement process, but typically having a high hydrogen to carbon, H/C weight ratio which results in a high heat-to-weight ratio and a clean burn. Cyclo-paraffins and aromatics reduce the H/C ratio and reduce the heat release per unit weight. The main advantage of the cyclo-paraffins is in that they reduce the fuel freeze point, which is a vital parameter for high altitude flight, whereas the aromatics (present between 8% and 25%) are important for gasket swelling purposes. Since aromatics are deficient in hydrogen, they have high heat content per unit volume, but lower heat content per unit mass compared to paraffins with the same carbon number. Jet fuel also contains trace amounts of sulphur, nitrogen and oxygen containing hydrocarbon compounds, which originate from the raw crude oil.

The composition of fossil and bio-jetfuels, from different feedstock and conversion techniques, have been investigated by e.g. Edwards *et al*., [3], Pires *et al*, [4], and Kang *et al*, [5]. Figures 1a, 1b and 1c show hydrocarbon distribution plots of Jet A, JP5 and JP8, respectively, showing some variations in hydrocarbon chain distribution. Jet A and JP5 has a wide distribution of carbon number from C6 to C17, with a dominant peak around C14, consisting primarily of iso-paraffins and n-paraffins with some naphtalenes and aromatics. Note however that JP8 does not include any n-paraffins and contains more lighter species than Jet A. Jet A and JP8 contain similar quantities of aromatics (around 14 vol%) whereas JP5 contain only around 3 vol% of aromatics. It is also vital to emphasize that the presence of olefins, hydrocarbons with double bonds, in jet fuels is undesirable as these are the most chemically reactive class of hydrocarbons.

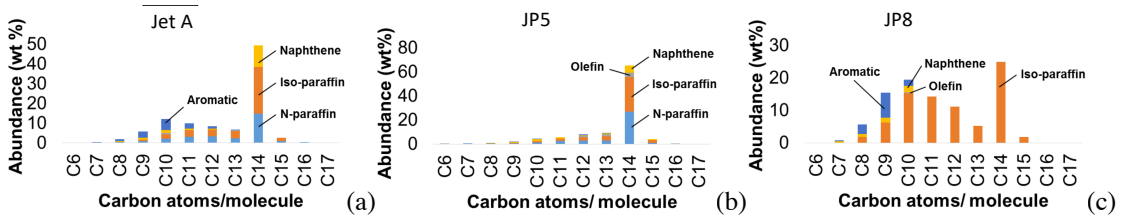

Figure 1. Hydrocarbon distribution plots of (a) Jet A, (b) JP5, and (c) JP8, from Pires *et al*, [4].

2.2. Sustainable Jet Fuels

Feedstocks for alternative jet fuels can be categorized by generations representing the sustainable development. **First-generation feedstocks** (1G) include edible food crops, such as oil palm, corn, sugarcane, sugar beets, and wheat, [6]. Sugar, starch, fat, and/or oil contents are extracted from these crops. Fats or oils can be easily converted to jet fuel through the Hydrogenated Esters and Fatty Acids (HEFA) process. Sugar or starch can be processed by the Direct Sugar to Hydrocarbon Conversion (DSCH) process whereas the Alcohol To Jet (ATJ) process is another technology for producing ethanol from corn. The main issues with the 1G feedstock is that it competes with food production, [7]. **Second-generation feedstocks** (2G) are fostered to avoid this issue, [8], and are classified into energy crops and waste biomass, with the latter being further classified into agricultural and forestry residues and food and municipal wastes. Regardless of classification, 2G feedstocks are either oil- or sugar-rich materials. However, in contrast to 1G crops, the sugars of 2G feedstocks are trapped in the tough and recalcitrant lignocellulosic matrix of plant cell walls that need pretreatment with enzymes/microorganisms and/or thermochemical transformations for biofuel conversion, [9]. The technical barriers and high costs of these conversion technologies are the main limitations of 2G feedstocks utilization. **Third Generation Feedstocks** (3G) include primarily algae and microalgae having virtually no food value, but having potentially high yields, virtually no land requirement, and relatively low-cost requirements, [10]. Algae and microalgae are capable of growing in water unsuitable for agriculture that can simultaneously lower operating costs and provide wastewater treatment benefit, [11]. **Fourth Generation Feedstocks** (4G) recognizes the potential of non-biological resources and genetically modified organisms, [8]. Non-biological feedstocks (e.g., CO_2, water, renewable electricity, and sunlight) may be the more en-

vironmentally benign option especially when flue gases from industrial plants are used. Genetically modified organisms (e.g., microalgae, cyanobacteria, fungi, and yeast) have artificially enhanced oil and/or sugar yields and negative carbon capabilities, which are mostly in the infancy stage of research. One direction is Power-to-Liquid (PTL) which involves the splitting of water into hydrogen and oxygen via a renewable- electricity-powered electrolyzer and then hydrogen is combined with CO_2/CO to produce alternative jet fuel, [12]. Another route is the use of concentrated solar energy in splitting water and CO_2 to produce syngas as precursor for alternative jet fuel production, [12]. When these technologies become mature, jet fuels from 4G feedstocks have the potential to become the most sustainable and economical sources.

Jet fuels from renewable sources has a different composition and in many cases show a much larger variation in composition than the fossil jet fuels, figure 1, depending on the different feedstocks and the conversion pathway(s). These compositions are not within the approved standards, and hence the renewable fuels are only accepted for use as drop-in fuels in the fossil jet fuel. To illustrate the variety of the composition of SAF, figure 2 show hydrocarbon distribution plots for Gevo ATJ, Sasol FT (Fischer Tropsch) synthetic kerosene, and Kior Hydrotreated Depolymerized Cellulosic Jet (HDCJ) – all being first generation SAF. Gevo ATJ and Sasol FT are mainly composed of paraffins, with low amounts of aromatics, naphtenes and olefins. Kior HDCJ is rich in aromatics and naphtenes, with very low content of paraffins. Since some of the SAFs tested contain lower levels of aromatics, they need to be blended with fossil jet fuels to reach the targeted level of aromatics to provide the acceptable swelling of gaskets. Several of the alternative jet fuels presented here do not have a balanced composition as such, and therefore they will persist a challenge to be used alone as fuel as their thermodynamic, spray and combustion properties also will be different as these quantities are highly dependent on the molecular composition.

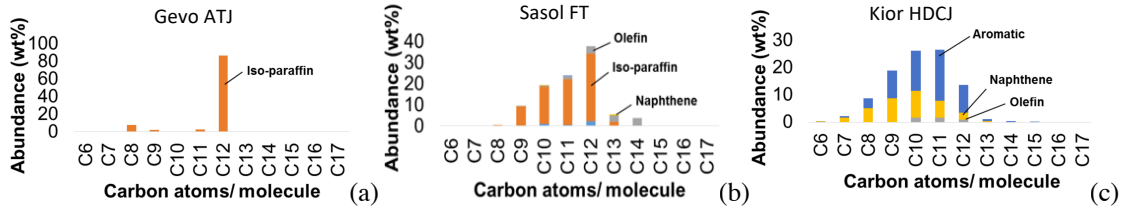

Figure 2. Hydrocarbon distribution plots of (a) Gevo ATJ, (b) Sasol FT and (c) Kior HDCJ, from Pires *et al*, [14].

2.3. Representative Category A, B and C Test Fuels

Based on requirements developed in the CRATCAF program, [13], the US NJFCP program, [14], defined a suite of conventional jet fuels and test jet fuels to characterize the sensitivity of combustion to fuel specifications. These fuels were developed by Air Force Research Laboratory's Fuels Branch in Dayton, Ohio, to span the full range of jet fuel composition and properties that could be encountered with conventional and alternative jet fuels. The fuels are grouped into three different categories: (i) Category A jet fuels are conventional fossil-based jet fuels such as Jet A, JP5 and JP8, (ii) Category B jet fuels are alternative jet fuels based on renewable sources but found to have unacceptable chemical, spray, and combustion properties, and (iii) Category C are alternative jet fuels purposely designed to explore the edges of the jet fuel composition-property space, such as fuels being at the viscosity limit of the specification or fuels whose composition is outside of the typical composition of conventional jet fuels of Category A. Table 1 lists a few selected Category A and Category C jet fuels in terms of their description, chemical formula, molar mass, M, lower heating value, LHV, and derived Cetane number, DCN. The DCN measures the ignition characteristics, with a higher DCN meaning that the fuel is easier to ignite. This will be further commented on in Section 2.4. The composition of the Category C fuels is often simpler than that of the Category A fuels and, although the LHV for all Category A and C fuels are similar the DCN spans a much wider range, from 17 for C1 to 50 for C2, revealing that these fuels may be both easier and harder to ignite than fossil jet fuels such as A2 or Jet A. The single-component fuels included here, n-heptane (C_7H_{16}) and n-dodecane ($C_{12}H_{26}$) have the same basic carbon chain

structure (n-paraffinic) but significant variation in the Cetane number, with 52 and 74 for the two fuels, respectively, facilitating investigating fuel flexibility in general.

Table 1. List of Category A and Category C jet fuels.

Name	*Common name*	*POSF#*	*Description*	*Chemical formula*	*M [kg/mol]*	*LHV [MJ/kg]*	*DCN*
A1	JP8	10264	low flash/viscosity/aromatics	$C_{10.8}H_{21.6}$	0.1519	43.2	38
A2	Jet A	10325	average/nominal properties	$C_{11.4}H_{21.7}$	0.1586	43.1	48
A3	JP5	10289	high flash/viscosity/aromatics	$C_{12.0}H_{22.3}$	0.1661	43.0	43
C1	Gevo ATJ	11498	C_{12} and C_{16} iso-paraffins	$C_{12.5}H_{27.1}$	0.1844	43.9	17
C2		12223	84 vol% C_{14} iso-paraffins and 16 vol% trimethyl-benzene	$C_{12.3}H_{24.5}$	0.1823	43.6	50
C5		12345	73 vol% C_{10} iso-paraffins and 27 vol% trimethyl-benzene with flat boiling curve	$C_{9.7}H_{18.7}$	0.1393	42.8	39
C6	Virent HDO SKA	10279	60 vol% cycloparaffins, 17% di-cyclo-paraffins, 10 vol% iso-paraffins and 8 vol% n-paraffins	$C_{11.9}H_{23.7}$	0.1683	43.6	37

2.4. Thermophysical Properties of Fossil and Sustainable Jet Fuels

The chemical composition of fossil and sustainable non-fossil jet fuels influences also the thermophysical properties together with the chemical kinetics and combustion behavior. Among all the physical properties that can be measured in order to provide a detailed thermophysical characterization of the jet fuel the flash point and the viscosity were recognized as the parameters exerting the greatest impact on the ignition and combustion behavior according to Edwards, [3]. Table 2 summarizes the main thermophysical properties of the selected Category A and Category C jet fuels studied specifically in the present project.

Table 2. Main thermophysical properties of selected Category A and C fuels.

Property	**Jet A (POSF 10325)**	**JP5 (POSF 10289)**	**C1 (POSF 11498)**	**C5 (12345)**
Density [kg/m^3]	803	827	760	769
Viscosity @ 20 °C [cSt]	4.5	6.5	4.9	1.9
Heat of combustion [MJ/kg]	43.1	43	~43.88	42.8
Freeze point [°C]	-51	-50	<-61	-56

3. Chemical Kinetics

The use of numerical simulations to predict turbulent combustion in jet engines relay heavily on the description of the chemical kinetics and the associated transport properties. In addition, extended information about the relation between fuel structure and combustion characteristics can be obtained from 0D and 1D simulations of ignition, oxidation, flame propagation and extinction. In this section we give an overview of the chemical mechanisms commonly used in numerical simulations of aviation fuels, and discuss the combustion chemistry of the different fuels.

3.1. Chemical Kinetics Mechanisms

As both fossil and alternative jet fuel have complex compositions, cf. figures 1 and 2, the number of chemical reaction steps and the number of species produced and destroyed during the conversion from the vaporized fuel to the final products, dominated by CO_2 and H_2O, are very large. For a well-defined jet fuel like Jet A the most detailed chemical reaction mechanisms are commonly 3-5 components mechanisms that consists of 20,000 to 50,000 reaction steps, e.g. [15]. These, so called, surrogate mechanisms include fuel molecules with different functionalities, representing groups of real fuel constituents like n- and iso-paraffins and aromatic compounds. Using such large comprehensive reaction mechanisms provides a detailed, realistic, and accurate description of the combustion process. Numerical simulations using such large reaction mechanisms can, unfortunately, only be performed for extremely simplified, canonical, situations to obtain for example the laminar flame speed, s_u, or the ignition delay time, τ_{ign}, of a fuel/air mixture. For num-

erical simulations of more realistic situations many other effects need to be considered like the combustor geometry, turbulence and vaporization, and in that case the reaction mechanism needs to be simplified. Reaction mechanisms with about 20 to 50 chemical species and from 50 to maybe 300 reactions can be used in LES, however at a large computational cost.

Simplified reaction mechanism can either be obtained by reducing the large comprehensive reaction mechanisms using mathematical methods or by constructing small comprehensive reaction mechanisms using a bottom-up approach. The most common reduction method is the Direct Relation Graph (DRG) method, which can often reduce a mechanism down to 10% of the original size. Considering the size of the original jet fuel mechanisms, tens of thousands as mentioned above, it is clear that a reduction down to about 10% of the original size is not sufficient.

Bottom-up methodologies have been more successful in production of very compact mechanisms and there are two such approaches available that have been applied to multiple kerosene-based jet fuels. Here, we use the approach proposed by Wang *et al.*, [16], who have developed small comprehensive reaction mechanisms for the three Category A fuels Jet A, JP5 and JP8, as well as for the two Category C fuels C1 and C5. The two reference fuels of interest in the present work, n-heptane and n-dodecane, have been modeled by Lu & Law, [17], and Yao *et al.*, [18], respectively using a method similar to that in [16].

3.2. Combustion Characteristics for Fossil- and Bio-aviation Fuels

Figure 3 compares predictions of the laminar flame speed, s_u, ignition delay time, τ_{ign}, and extinction strain-rate, σ_{ext}, for n-heptane, n-dodecane, Jet A, JP5, C1 and C5 with experimental data, [19-27], where available. Laminar flames are simulated at 1 atm at equivalence ratios from 0.6 to 1.6 to extract the laminar flame speed and the temperature trends. The σ_{ext} computation is done using a counterflow diffusion flame at atmospheric pressure and temperatures of 473 K and 300 K for the fuel and the oxidizer, respectively. The ignition delay time is computed for 10 atm of pressure at stochiometric equivalence ratio, with corresponding experimental results gathered for stoichiometric mixtures between $p = 12$ atm and 14.80 atm.

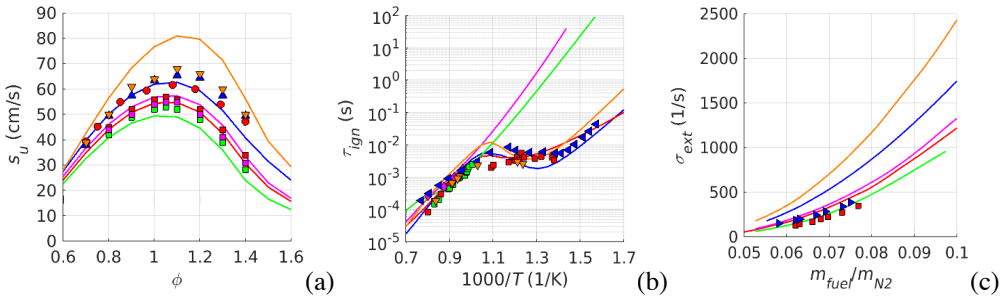

Figure 3. (a) Laminar flame speed (s_u), (b) ignition delay time (τ_{ign}), and (c) extinction strain rate (σ_{ext}), for n-dodecane (—), n-heptane (—), Jet A (—), C1 (—) and C5 (—). Lines denote the numerical predictions while symbols the experimental data from Kumar *et al.*, [19-20], (▲, ▲), Xu *et al.*, [21], (■, ■), Kumar *et al.*, [22], (●), Liu *et al.*, [23], (▶), Mao *et al.*, [24], (◀), Movaghar *et al.*, [25], (■), Davidson *et al.*, [26], (◆), and Shen *et al.*, [27], (▼).

The laminar flame speed, s_u, figure 3a, shows that the predictions from the small comprehensive reaction mechanisms agree well with the experimental results from Kumar *et al.*, [19], Xu *et al.*, [21], and Movaghar *et al.*, [25]. The largest deviations are observed for the reference fuels n-heptane and n-dodecane, which is most likely due to the simplified sub-mechanisms for C_5-C_{12} species, which is somewhat improved in the reaction mechanisms for Jet A, C1 and C5 as these mechanisms are more recently developed. Despite differences in lower heating value between n-heptane, n-dodecane, Jet A, C1 and C5, the flame temperature (not shown) only differs by ~20 K at most. Regarding the ignition delay time, τ_{ign}, in figure 3b, all fuels behave similarly in the high-temperature regime, showing qualitatively good agreement between simulations and experiments. A well-defined Negative Temperature Coefficient (NTC) plateau characterizes τ_{ign} for n-heptane, n-dodecane and Jet A but cannot be observed for C1 and C5. This plateau is closely

associated with the derived Cetane number mentioned previously. Regarding the extinction strain rate, σ_{ext}, in figure 3c we find that the simulations predict a higher resistance to extinction for n-dodecane, C5, Jet A and then C1. The predictions for n-dodecane and Jet A overestimate the strain rates when compared with the experimental results from Xu *et al*., [21], and Liu *et al*., [23]. The disagreement for n-dodecane is larger than the discrepancies for Jet A. Extinction strain rate is not only dependent on the chemical reactions but also on transport properties, which are not very well determined for many heavy fuel molecules. Discrepancies in extinction strain rates could therefore come from either the transport properties or the chemical reactions, and regarding the chemical reactions it is not fully understood whether it is the fuel breakdown reactions or the reactions later in the oxidation chain that could be faulty. While laminar flame speed and ignition are fairly well understood, further research is needed related to extinction strain rate.

4. Computational Combustion Modeling

Combustion is governed by the basic transport equations of fluid dynamics and heat transfer with additional models for combustion chemistry, radiative heat transfer, and other important sub-processes such as spray break-up and vaporization (when appropriate). Jet engine and gas turbine combustion are generally highly turbulent, and the fuel is most often injected separately, either far upstream of the flame, resulting in a premixed flame, or just upstream of the flame, resulting in a non-premixed (or diffusion flame). In these engines the fuel is often liquid and in that case the liquid stream is often discharged into the combustion chamber in the form of a spray of droplets that vaporize prior to combustion. Computational models for turbulent (spray) combustion are thus composed of several interacting components centered around a set of balance equations, complemented by models for the spray, turbulence, combustion chemistry, and turbulence chemistry interactions as will be briefly outlined in the following.

Modeling turbulent combustion requires solving transport equations for mass, momentum and energy supplemented with transport equations for the individual species concentrations. The full set of transport equations then consists of 5+N partial differential equations, where N is the number of species in the reaction mechanism, describing both laminar and turbulent flow and combustion. Turbulent flow includes a wide range of spatial eddy scales, ranging from the largest integral scales to the smallest turbulent (Kolmogorov) scales, with the latter being 1000 to 10,000 times smaller than the former. This wide gap in scales makes numerical simulations very challenging since the computational grid can usually not be made fine enough to resolve the smallest Kolmogorov scales. Instead we typically use turbulence modeling methods which task is to resolve the largest scales and model the effects of the smallest scales on the resolved scales. During the past decade Large Eddy Simulation (LES), [28-30], which is a compromise between Direct Numerical Simulation (DNS), [31], in which all scales are resolved, and Reynolds Averaged Navier-Stokes (RANS) methods, [32], in which all scales are modeled, has been extensively used to study combustion applications, [35-37]. In LES, turbulent scales larger than the grid spacing are resolved, whereas subgrid scales, and the effect they have on the larger scales, is modeled. This allows for capturing transient phenomena such as thermoacoustic oscillations, lean blow out etc. The influence of the subgrid turbulence is in the present work modeled using the Localized Dynamic K equation subgrid Model (LDKM), [38], whereas the subgrid turbulence chemistry interactions are modeled using the Partially Stirred Reactor (PaSR) model, [39], both used in the recent past with good to excellent agreement with reference data, [33-37]. Separate models for the spray, using Lagrangian particles, representing the atomizing and vaporizing droplet clouds, producing gaseous fuel species that participate in the gas-phase combustion chemistry.

The LES equations are solved using a finite volume-based code developed from the OpenFOAM C++ library, [40], which in turn is based on an unstructured collocated finite volume method using Gauss's theorem. The time-integration is performed with a semi-implicit second order accurate two-point backward differencing scheme, [41], for premixed flames and the single-point implicit Euler scheme for spray flames. The convective fluxes are reconstructed using multi-dimensional cell limited linear interpolation, whereas diffusive fluxes are reconstructed using a

combination of central difference approximations and gradient face interpolation. Here, a compressible version of the Pressure Implicit with Splitting of Operators (PISO) method, [42], is used to discretize the pressure-velocity-density coupling, using the thermal equation of state. The combustion chemistry is integrated separately, using a Strang-type operator-splitting algorithm, [43], and a Rosenbrock time-integration scheme, [44-45], for the resultant system of differential equations. The algorithm is second order accurate in both space and time, and the equations are solved sequentially with a Courant number limitation of approximately 0.5.

5. Results from CFD Studies

In this project we have considered three different turbulent flame configurations, selected based on the need to simulate various aspects of the combustion process. In order of increasing complexity these consist of the Cambridge burner, which is a medium size prevaporized laboratory flame, the AFRL burner, which is a large size prevaporized laboratory flame, and the Timecop burner which is a large size spray combustor similar to that of a jet engine. These three configurations have to different extents been used in experimental studies on relevant fuels, which allow validation of the computational models. Below results from the three cases are briefly reviewed and summarized.

5.1. Cambridge Burner

In the experimental study of Pathania *et al*., [46], ethanol, n-heptane, Jet A, and C1 were all tested in a pre-vaporized premixed axisymmetric bluff-body stabilized flame. In [42] we report numerical simulations at $\phi/\phi_{LBO} = 1.2$, where ϕ_{LBO} is the equivalence ratio at lean blow-off of n-heptane, Jet A, and C1, all showing good overall agreement between experiments and modeling predictions. The supply pipe and burner section are fully resolved, and discharge into a large cylindrical domain with a length of $8.5d$, and a radius of $3.9d$, where d is the bluff-body diameter A grid is positioned at the inlet of the pipe section to trigger large-scale turbulence, which on average contributes 84% of the total turbulent kinetic energy in the whole domain, and >90% in the flame. Hexahedral grids of 4.0 and 16.8 million cells are used to discretize the domain. The inlet mass-flow is selected to achieve a bulk exit velocity of $u_b = 23.5$ m/s, corresponding to a Reynolds number of *Re*=25,000. Figure 4 presents a schematic of the burner together with a volumetric rendering of the instantaneous temperature for conventional Jet A.

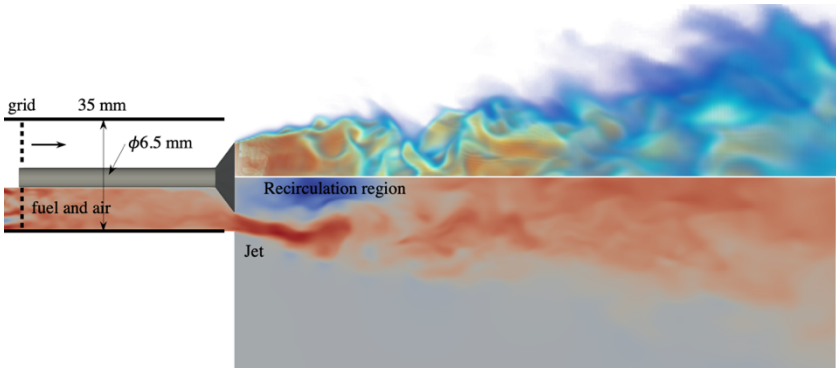

Figure 4. Volume rendering of temperature, T (upper part of figure), and the axial velocity, v_x (lower part of figure), with a schematic of the burner as modeled in the simulations. Red colors represent high values and blue colors represent low values.

The axial velocity, v_x, reveals a recirculation region just downstream of the bluff body and higher velocities surrounding the recirculation regions. The recirculation region pulls back hot combustion products from downstream towards the bluff body increasing the residence time, making sure combustion is completed, at the same time as the shear layers trailing off the bluff-body are heated from within, guaranteeing flame stabilization. The temperature, T, remains high

in the recirculation region, whereas further downstream both v_x and T gradually becomes more and more fragmented, or turbulent, due to the Kelvin-Helmholz shear layer instabilities and the Bénard von Karman convective instabilities. Due to entrainment of cold surrounding air the high temperature in the recirculation region gradually cool with increasing distance from the bluff body. For all four experimentally investigated fuels, Jet A, ethanol, n-heptane and C1, good agreement between the time-averaged axial velocity distribution, $\langle v_x \rangle$, and the time-averaged OH distribution, $\langle Y_{OH} \rangle$, from the numerical simulations are observed. For details see [47]. It is thus established that the simulation model can capture the flow provided that the chemical reaction mechanism can accurately represent the fuel combustion chemistry.

Figure 5 compare instantaneous and time-averaged CH_2O-PLIF (Planar Laser Induced Fluorescence) images from the experiments with results from the numerical simulations. CH_2O is produced in the low temperature oxidation process and consumed in the high temperature oxidation process, and is thus a good marker for the flame, demarcating the outer, cold, reactant zone from the inner, hot, product zone. Good agreement between both the instantaneous and time-averaged CH_2O-PLIF distributions can be observed, revealing a highly wrinkled flame zone that is sufficiently well resolved by the numerical simulations. Similar differences between the fuels can be observed in the experiments and simulations, with C1 showing the most wrinkled flame with also the highest concentrations of CH_2O. More interestingly is that the averaged CH_2O profiles from both the experiments and the numerical simulations for CH_2O are thinner than those of Jet A and heptane, whereas their laminar counterparts show similar thicknesses. This suggest that C1 is differently affected by the turbulence than Jet A and heptane, and that the HyChem reaction mechanisms can accurately capture this. However, the underlaying mechanism is not fully understood and this topic is an important trend to understand, beyond the present project.

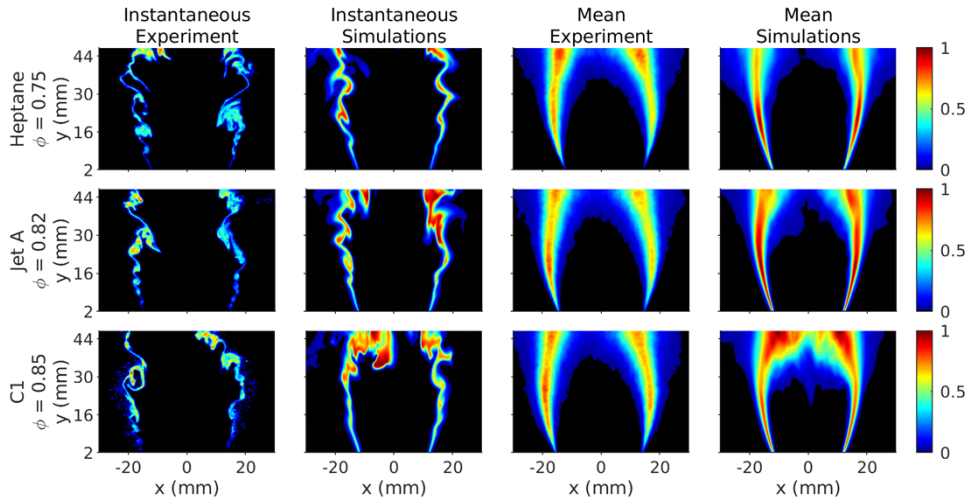

Figure 5. Instantaneous and time-averaged CH_2O-PLIF distributions from the experiments of Pathania *et al*, [41], and from the numerical simulations downstream of the bluff-body.

5.2. AFRL Burner

Next, we consider n-dodecane, Jet A, C1 and C5 combustion in the equilateral triangular bluff-body combustor of Air Force Research Laboratory, Wright-Patterson Air Force Base, [48], shown in figure 6. High temperature air is generated by an electrical heater combined with a vitiator to provide the airstream in which liquid fuel is injected through the fuel spray bars located vertically just downstream of the critical plate, acoustically isolating the test section from the supply section. The test section is rectilinear with a cross-section of 152.4×127.0 mm^2. The bluff body is a solid 38.1 mm equilateral triangle, and the test section exit is open to the atmosphere. Sixteen high-frequency pressure transducers, mounted in a semi-infinite tube configuration, are positioned along the streamwise and transverse directions. Planar Laser-Induced Fluorescence (PLIF) is per-

formed to evaluate the fuel-air pre-mixedness at $x = -4H$, and high frequency OH*-chemiluminescence imaging is performed to characterize the flame. Experimental pressure fluctuations and OH chemiluminescence images are available for n-dodecane, Jet A, and C1, [48], for comparison with numerical simulation results. These comparisons show qualitative and quantitative agreement, and that the numerical simulations captures the fuel sensitivities.

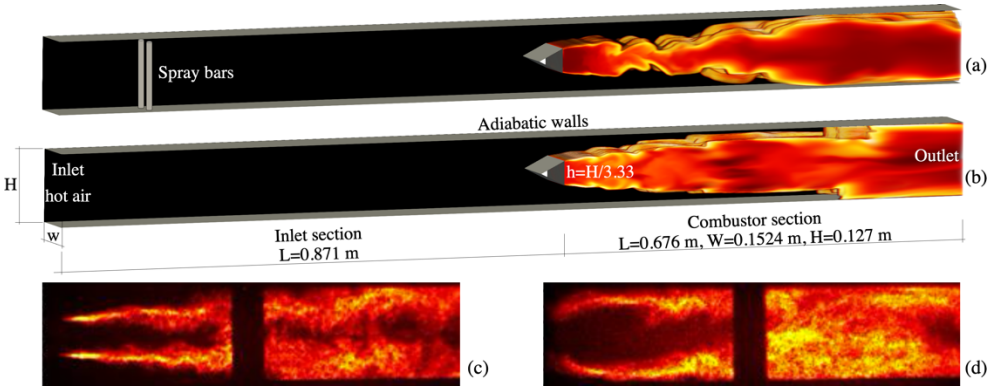

Figure 6. Isometric views of the AFRL bluff body combustor, [48], in terms of OH chemiluminescence for n-dodecane at equivalence ratios of (a) ϕ=0.66 and (b) 0.87, together with line-of-sight averaged experimental OH chemiluminescence images at (c) ϕ=0.66 and (d) 0.87, respectively.

Figure 6 shows isometric views of the AFRL equilateral triangular bluff body combustor, [48], in terms of OH chemiluminescence for n-dodecane at equivalence ratios of (a) ϕ=0.66 and (b) 0.87, together with line-of-sight averaged experimental OH chemiluminescence images at (c) ϕ=0.66 and (d) 0.87, respectively. Both the numerical simulations and the experiments reveal a significant influence of the equivalence ratios, ϕ, with the ϕ=0.66 flame being more narrow, due to the lower laminar flame speed, s_u, and composed of two separate flame brushes. The ϕ=0.87 flame is wider, due to higher s_u, and shows two flame brushes that initially do not interact. Further downstream, the flame brushes in the ϕ=0.66 case widen, approach each other, start to interact while also developing ondulating movements. In the ϕ=0.87 case the flame brushes start to interact, and merge completely. Vortex induced mixing, baroclinic torque and exothermicity play a key role in developing these two flame topologies. The fuel chemistry is primarily responsible for the exothermicity, and as will be evident from figure 7, different fuels behave differently.

Figure 7 presents comparisons of the time-averaged temperature, $\langle\tilde{T}\rangle$, and temperature fluctuation, T^{rms}, profiles at $x/h = 0.375, 0.95, 1.53, 3.75$, and 9.40, normalized by the adiabatic flame temperature, T_{ad}, from the numerical simulations of dodecane, Jet A, C1 and C5, at $\phi = 0.66$. For $\langle\tilde{T}\rangle$ we find that at $x/h = 0.375$ all fuels result in similar $\langle\tilde{T}\rangle$ profiles but with C5 showing a marginally lower peak temperature. For $x/h = 0.95$, C5 clearly shows a lower peak temperature but also a wider, more diffusive, $\langle\tilde{T}\rangle$ profile. At the end of the recirculation bubble, at $x/h \approx 1.53$, the observed differences noted earlier have amplified, so that the $\langle\tilde{T}\rangle$ profile of C5 is lower and wider than those of the other fuels. The n-dodecane $\langle\tilde{T}\rangle$ profile follows next, whereas there is almost no difference between the $\langle\tilde{T}\rangle$ profiles of Jet A and C1. In the recovery region, at

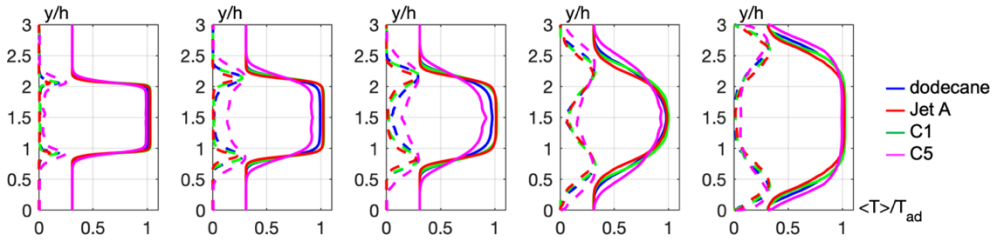

Figure 7. Comparison of time-averaged temperature, $\langle\tilde{T}\rangle$, (solid lines) and rms temperature fluctuations, T^{rms}, (dashed lines) at $x/h = 0.375, 0.95, 1.53, 3.75$, and 9.40, from left to right, between LE simulations of dodecane, Jet A, C1 and C5, at an equivalence ratio of $\phi = 0.66$.

$x/h \approx 3.75$, all $\langle \widetilde{T} \rangle$ profiles are wider and smoother, with that of C5 being the widest and that of Jet A being the narrowest. In the fully developed turbulent combustion region, at $x/h \approx 9.40$, the ordering is the same, but the differences are now less significant. For T^{rms} we find that although the T^{rms}-profiles are similar, the fluctuation levels of C5 are higher in the recirculation bubble, and particularly towards the end of the recirculation bubble. For the other fuels the T^{rms}-profiles are virtually identical, suggesting that these fuels have similar flame dynamics.

Comparing wall-pressure fluctuations, p^{rms}, along the upper combustor wall between experimental data and simulation results show good agreement, and also that p^{rms} increase monotonically with the equivalence ratio, ϕ, but differently for different fuels. Jet A and dodecance show a similar and gradual increase in p^{rms} with increasing ϕ, whicle C1 and C5 both show a sharper increase in p^{rms} occurring at a higher equivalence ratios

5.3. TIMECOP Burner

The final simulation case presented in this report is based on a test rig studied at DLR Institute of Propulsion Technology, [49-50]. Numerical studies of this case have previously been carried out with LES, [51-52], SAS, [52], and RANS, [53]. With a length of 0.264 m and a square cross section of 102×102 mm^2, the combustor is designed to be an appropriate representative of a single-sector aeroengine combustor with liquid fuel injection. The combustor is presented in figure 9, together with some key results to visualize the flow and combustion. Air is supplied to a burner equipped with two co-rotating swirlers, which cause the air flow to swirl about the central axis. Liquid kerosene is injected along the inner burner wall just upstream of the combustion chamber. At the end of the pre-filmer lip, the liquid film is atomized by the rotating air flow, causing the fuel to enter the combustor as a cone-shaped cloud of dispersed droplets. The swirlers give rise to a flow pattern inside the combustor that consists of a Central Recirculation Zone (CRZ) enveloped by a Main Flow Cone (MFC), with primarily axial flow, and an Outer Recirculation Zone (ORZ) is formed near the corners of the combustor base. The fuel quickly evaporates and ignites in the MFC due to the high temperature, and the resulting flame is kept stable near the inner shear layer that forms the highly turbulent boundary between the CRZ and the MFC. Hot combustion products are recirculated towards the spray, continuously heating it.

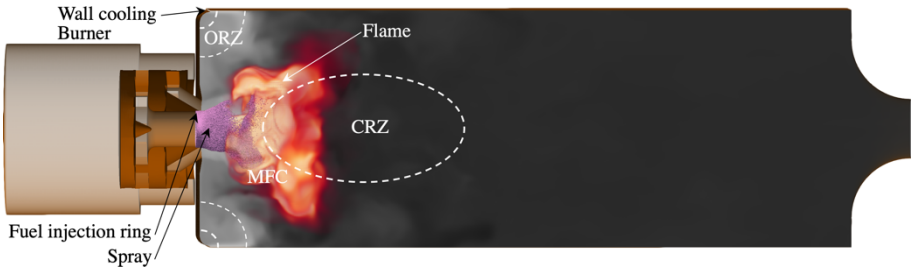

Figure 9. Centrally cut geometry with LES results for Jet A. Inlets are green, and walls are colored by time-averaged temperature. The spray is colored in magenta, and the time-averaged flame is colored in light red. Arrows indicate mean velocity direction in the central plane inside the Main Flow Cone (MFC). The central (CRZ) and outer (ORZ) recirculation zones are denoted by white contours.

The Timecop test rig has been operated with pressures, temperatures and mass flows that represent both idle and cruise conditions in a typical aeroengine. For idle conditions the air pressure is 4 bar, the air preheat temperature is 550 K, the burner air mass flix is 60 g/s, the cooling air mass is 17 g/s and the liquid fuel mass flux is 3.0 g/s. For cruise conditions the air pressure is 10 bar, the air preheat temperature is 650 K, the burner air mass flix is 140 g/s, the cooling air mass is 39 g/s and the liquid fuel mass flux is 6.8 g/s. Experiments have been performed with Jet A, whereas we have performed numerical simulations with Jet A for validation, and with JP5, C1 and C5 in order to examine the differences caused by different fuels.

Figure 10 show comparisons between the different fuels and between the experiments (using Jet A) and the numerical simulations at the two operating conditions (idle and cruise) with the four different fuels. Based on the spray and volumetric renderings in the upper panels of figure 4

we find that the flames behave similarly, with a gaseous fuel cloud developing around the spray, outside of which the heat release takes place. It appears that the heat release is primarily occurring in the premixed mode; the fuel and oxidizer are mixed before combustion, which means that the gradients of their mass fractions are parallel across the flame front. Comparing the flame shapes in terms of time-averaged OH chemiluminescence images between the experimental results and the numerical simulations for Jet A at both idle and cruise conditions show good overall agreement for both idle and cruise, revealing the ability to capture the behavior of both modes. The influence of the fuels is also very clear, with JP5 being significantly more sensitive to time-averaged thermoacoustic instabilities compared to Jet A, and thus showing a different OH chemiluminescence distribution at cruse conditions, C1 showing more heat release along the inner shear layer, and C5 showing a significantly larger lift-off at idle condition and similarity with JP5 at cruise conditions. These results clearly indicate a significant fuel sensitivity.

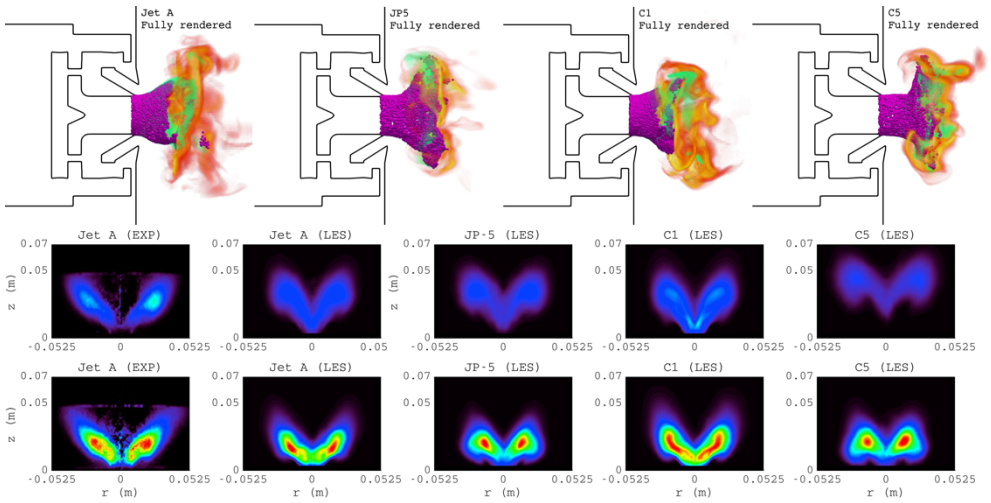

Figure 10. Upper four panels present snapshots of the simulated spray flame colored by the heat release together with the spray in magenta and gaseous fuel in green. The middle four panels show OH chemiluminescence images from the experiment, and simulations using Jet A, JP5, C1 and C5 whereas the lower four panels show OH chemiluminescence images from the experiment, and simulations using Jet A, JP5, C1 and C5. The experimental results taken from [50].

5. Concluding Remarks

The aim of this report was to give an overview of jet fuel properties and combustion characteristics, with focus on similarities and differences between fossil fuels and selected bio-jetfuels. A first finding is that the numerical modeling is validated against experimental data, where available, with good agreement. In general, there is a lack of experimental data to validate the numerical simulations against, in particular data for bio jet fuels. Within the recently initiated competence center CESTAP (Competence cEntre in Sustainable Turbine fuels for Aviation and Power) experimental work will provide additional validation data that also can be used for physics elucidation. From the chemical kinetics modeling it is apparent that the ignition and flame propagation behavior is significantly different for different fossil and non-fossil fuels, as an example the laminar flame speed of the bio jet fuels C1 and C5 are lower than of Jet A whereas that of HEFA is higher. For the ignition delay time and extinction strain rate there is need for further validation and development of chemical kinetic mechanisms for accurate prediction of these properties for the novel fuels, but already the existing mechanisms show significant differences. These quantities are generally more important for gas turbine and jet engine combustion than the laminar flame speed as these combustors are usually spray combustors resulting in complex flame with a dominant non-premixed character.

The numerical simulations generally provide a cost effective approach to investigate vari-

ous aspect of combustion. This is particularly evident with modern high fidelity LES-based simulation models employing various finite rate chemistry models in which the combustion chemistry is directly coupled to the flow and solved for using numerical methods that can manage the very short time scales involved in the chemistry species transformation. As seen, and commented on, we find for all three cases investigated that the sensitivity to the fuel is significant. The quality of the results will therefore sensitive to which reaction mechanism is used to represent the combustion process, and hence carefully validated reaction mechanism of the same family are used to minimize systematic influences. The general results from the numerical simulation study is somewhat more complex than hoped for, but hence reflect our present lack of understanding of how the physics and chemistry of turbulent flames behaves. For the Cambridge burner similar flames are obtained by n-heptane, Jet A and C1, being in good agreement with the experimental results. A particular feature that the simulations recover is that the formaldehyde (CH_2O) layer is noticeably thinner for C1 compared to Jet A and n-heptane. This is not yet well understood but is believed to be an effect of turbulence, acting differently on different fuels. The C1 flame is also closer to blow-off, and is thus more sensitive to turbulent fluctuations. This is possibly due to the comparatively low Cetane number. For the bluff-body AFRL flame we also find good agreement with the experimental data, with the numerical simulations capturing the observed influence of different equivalence ratios, and the increased sensitivity of C1 to thermoacoustic instabilities. For this case we also find that C5 is sensitive to strong turbulent fluctuations and mixing in the internal shear layers, whereas dodecane, having a high Cetane number, is rather insensitive to turbulence. For the Timecop combustor the spray characteristics also play a role, with atomization and vaporization performing differently for different fuels. The spray flames for Jet A and C1 appear quite similar, and agree very well with the Jet A experiments. The JP5 and C5 flames also appear quite similar, revealing a different flame character, that we currently attribute to the different gas phase combustion reactions taking place downstream of the spray.

6. Publications

Åkerblom A.; 2022, "The Impact of Reaction Mechanism Complexity in LES of Liquid Kerosene Spray Combustion". 33rd Congress of the International Council of the Aeronautical Sciences.

Åkerblom A., Pignatelli F. & Fureby C.; 2022, "Gas Turbine and Jet Engine Combustion", Aerospace, **9**, p 838.

Pignatelli F., Passad M., Åkerblom A., Nilsson T., Nilsson E.J.K. & Fureby C.; 2022, "Predictions of Spray Combustion using Conventional Category A Fuels and Exploratory Category C Fuels", AIAA-2023-1486.

Fureby C.; 2022, "Paving the Route Towards Green Aviation with Hydrogen and Biojetfuels – A Numerical Study using OpenFOAM", Webinar: OpenFOAM in Combustion Research, Eds. Zhang H., Han W., Li S., Zhang J. & Fang L.

Åkerblom A. & Fureby C.; 2023, "LES Spray Combustion Modeling of the DLR Generic Single-Cup Combustor", Submitted to Flow, Turb. & Comb.

References

[1] CRC, Handbook of Aviation Fuels, Society of Automotive Engineers, 2004.

[2] Maurice L.Q., Lander H., Edwards T. & Harrison W.E.; 2001, "Advanced Aviation Fuels: A Look Ahead via a Historical Perspective", Fuel, 80, p 747.

[3] Edwards T.; 2017, "Reference Jet Fuels for Combustion Testing", AIAA 2017-0146.

[4] Pires A.P.P., Han Y., Kramlich J. & Garcia-Perez M.; 2018, "Chemical Composition and Fuel Properties of Alternative Jet Fuels", BioResources, **13**, p 2632.

[5] Kang D., Kim D., Kalaskar V., Violia A. & Boehman A.L.; 2019, "Experimental characterization of jet fuels under engine relevant conditions – Part 1: Effect of chemical composition on autoignition of conventional and alternative jet fuels", Fuel, **239**, p 1388.

[6] Lee R.A. & Lavoi J.M.; 2013, "From first- to third-generation biofuels: challenges of producing a commodity from a biomass of increasing complexity". Anim. Front., **3**, p 6

[7] Moioli E., Salvati F., Chiesa M., Siecha R. T., Manenti F. & Laio F.; 2018, "Analysis of the current world biofuel production under a water-food-energy nexus perspective". Adv. Water Resour. **121**, p 22
[8] Alalwan H.A., Alminshid A.H. & Aljaafari H.A.S.; 2019, "Promising evolution of biofuel generations". Subject review. Renew. Energy Focus, **28**, p 127.
[9] Boichenko S., Oksana V. & Anna, I.; 2013, "Overview of innovative technologies for aviation fuels production", Chem. Chem. Technol., **7**, p 305
[10] Cheng J.J. & Timilsina G.R.; 2011, "Status and barriers of advanced biofuel technologies: a review", Renew. Energy, **36**, p 3541
[11] Acheampong M., Ertem F.C., Kappler B. & Neubauer P.; 2017, "In pursuit of sustainable development goal (SDG) number 7: will biofuels be reliable?", Renew. Sustain. Energy Rev., **75**, p 927
[12] Richter S., Braun-Unkhof, M., Naumann C. & Riedel, U.; 2018, "Paths to Alternative Fuels for Aviation". CEAS Aeronaut. J., **9**, p 389.
[13] Edwards T., Moses C. & Dryer F.; 2010, "Evaluation of Combustion Performance of Alternative Aviation Fuels", AIAA 2010-7155.
[14] Colket M., Heyne J., Rumizen M., Gupta M., Edwards T., Roquemore W.M., Andac R., Boehm R., Lovett J., Williams R., Condevaux R., Turner D., Rizk N., Tishkoff J., Li C., Moder J., Friend D. & Sankaran V.; 2017, "Overview of the National Jet Fuels Combustion Program", AIAA J., **55**, p 1087.
[15] http://creckmodeling.chem.polimi.it/menu-kinetics/menu-kinetics-detailed-mechanisms
[16] Wang H., Xu R., Wang K., Bowman C.T., Davidson D.F., Hanson R.K., Brezinsky K. & Egolfopoulos F.N.; 2018, "A Physics-Based Approach to Modeling Real-Fuel Combustion Chemistry - I. Evidence from Experiments, and Thermodynamic, Chemical Kinetic and Statistical Considerations", Comb. Flame, **193**, p 502.
[17] Lu T. & Law C.K.; 2008, "Strategies for Mechanism Reduction for Large Hydrocarbons: n-heptane", Comb. Flame, **154**, p 153.
[18] Yao T., Pei Y., Zhong B.-J., Som S., Lu T. & Luo K.H.; 2017, "A Compact Skeletal Mechanism for n-dodecane with Optimized Semi-Global Low-Temperature Chemistry for Diesel Engine Simulations", Fuel, **191**, p 339.
[19] Kumar K. & Sung C.-J.; 2007, "Laminar Flame Speeds and Extinction Limits of Preheated n-decane/O2/N2 and n-dodecane/O2/N2 Mixtures", Comb. Flame, 151, p 209.
[20] Kumar K., Freeh J., Sung C.-J. & Huang Y.; 2007, "Laminar Flame Speeds of Preheated iso-Octane/O2/N2 and n-Heptane/O2/N2 Mixtures", J. Prop.. Power, 23, p 428.
[21] Xu R., Wang K., Banerjee S., Shao J., Parise T., Zhu Y., Wang S., Movaghar A., Lee D.J., Zhao R., Han X., Gao Y., Lu T., Brezinsky K., Egolfopoulos F.N., Davidson D.F., Hanson R.K., Bowman C.T. & Wang H.; 2018, "A Physics-Based Approach to Modeling Real-Fuel Combustion Chemistry – II. Reaction Kinetic Models of Jet and Rocket Fuels", Comb. Flame, 193, p 520.
[22] Kumar K., Sung C.-J. & Hui X.; 2011, "Laminar Flame Speeds and Extinction Limits of Conventional and Alternative Jet Fuels", Fuel, 90, p 1004.
[23] Liu S., Zhao R., Xu R., Egolfopoulos F.N. & Wang H.; 2017, "Binary Diffusion Coefficients and Non-Pre- mixed Flames Extinction of Long-Chain Alkanes", Proc. Comb. Inst., 36, p 1523.
[24] Mao Y., Raza M., Zhiyong W., Jizhen Z., Liang Y., Wang S., Zhu L. & Xingcai L.; 2020, "An Experimental Study of n-dodecane and the Development of an Improved Kinetic Model", Comb. Flame, 212, p 388.
[25] Movaghar A. & Egolfopoulos F.N.; 2017, personal communication.
[26] Davidson D.F., Zhu Y., Shao J. & Hanson R.K.; 2016, personal communication.
[27] Shen H.-P., Steinberg J., Vanderover J. & Oehlschlaeger M.; 2009, "A Shock Tube Study of the Ignition of n-Heptane, n-Decane, n-Dodecane, and n-Tetradecane", Energy Fuels, 23, p 2482.
[28] Sagaut P.; 2001, "Large Eddy Simulation for Incompressible Flows", Springer Verlag.
[29] Menon S. & Fureby C.; 2010, "Computational Combustion", In Encyclopedia of Aerospace Engineering, Eds. Blockley R. & Shyy W., John Wiley & Sons.
[30] Echekki T. & Mastorakos E.; 2011 (Eds.), "Turbulent Combustion Modeling", Fluid Mechanics and its Applications, 95, Springer Science+Business Media.
[31] Hawkes E.R., Sankaran R., Sutherland J.C. & Chen J.H.; 2005, "Direct Numerical Simulation of Turbulent Combustion: Fundamental Insights Towards Predictive Models", J. Physics: Conference Series, **165**, p 65.
[32] Guiterrez L.F., Tamagno J.P. & Elaskar S.A.; 2016, "RANS Simulation of Turbulent Diffusive Combustion using OpenFoam", J. Appl. Fluid Mech., **9**, p 669.
[33] Jones W.P., Marquis A-J. & Wang F.; 2015, "Large Eddy Simulation of a Premixed Propane Turbulent Bluff Body Flame using the Eulerian Stochastic Field Method", Fuel, **140**, p 514.

[34] Fureby C., Zettervall N., Kim S. & Menon S.; 2015, "Large Eddy Simulation of a Simplified Lean Premixed Gas Turbine Combustor", 9th Int. Symp. on Turbulence and Shear Flow Phenomena (TSFP-9), Melbourne, Australia.
[35] Fedina E., Fureby C., Bulat G. & Maier W.; 2017, "Assessment of Finite Rate Chemistry Large Eddy Simulation Combustion Models", Flow, Turb. and Comb., **99**, p 385.
[36] Fureby C.; 2018, "The Volvo Validation Rig – A Comparative Study of Large Eddy Simulation Combustion Models at Different Operating Conditions", AIAA 2018-0149.
[37] Nilsson T., Zhong S. & Fureby C.; 2021, "LES of H_2-air Jet Combustion in High Enthalpy Supersonic Crossflow", Phys. Fluids, **33**, p 035133.
[38] Kim W.-W. & Menon S.; 1995, "A New Dynamic One Equation Subgrid-scale Model for Large Eddy Simulations", AIAA 95-0356.
[39] Sabelnikov V. & Fureby C.; 2013, "LES Combustion Modeling for High Re Flames using a Multiphase Analogy", Comb. Flame, **160**, p 83.
[40] Weller H.G., Tabor G., Jasak H. & Fureby C.; 1997, "A Tensorial Approach to CFD using Ob¬ject Oriented Techniques", Comp. in Physics, **12**, p 629.
[41] Lambert, J. D.; 1973, "Computational Methods in Ordinary Differential Equations", New York, Wiley.
[42] Issa, R.I.; 1986, "Solution of the Implicitly Discretized Fluid Flow Equations by Operator Splitting", J. Comp. Phys., **62**, p 40.
[43] Strang, G.; 1968, "On the Construction and Comparison of Difference Schemes", SIAM J. Numerical Analysis, **5**, p 506.
[44] Rosenbrock H.H.; 1963, "Some General Implicit Processes for the Numerical Solution of Differential Equations", The Computer Journal, **5**, p 329.
[45] Hairer, E. & Wanner, G.; 1991, "Solving Ordinary Differential Equations II Stiff and Differential-Algebraic Problems", 2nd Ed., Springer Verlag, Berlin Heidelberg.
[46] Pathania R.S., Skiba A.W. & Mastorakos E.; 2021, "Experimental Investigation of Unconfined Turbulent Premixed Bluff-body Stabilized Flames Operated with Vapourised Liquid Fuels", Comb. Flame, **227**, p 428.
[47] Åkerblom A., Pignatelli F. & Fureby C.; 2022, "Gas Turbine and Jet Engine Combustion", Aerospace, **9**, p 838.
[48] Paxton B.T., Fugger C.A., Tomlin A.S. & Caswell A.W.; "Experimental Investigation of Fuel Type on Combustion Instabilities in a Premixed Bluff- Body Combustor", AIAA 2020-0174.
[49] Behrendt T., Frodermann M., Hassa C., Heinze J., Lehmann B. & Stursberg K.; 1999, "Optical Measurements of Spray Combustion in a Single Sector Combustor from a Practical Fuel Injector at Higher Pressures". Symp. on Gas Turbine Engine Combustion, Emissions and Alternative Fuels.
[50] Meier U., Heinze J., Freitag S. & Hassa C.; 2012, "Spray and Flame Structure of a Generic Injector at Aero-engine Conditions", J. Eng. For Gas Turbines and Power, **134**, p 031503.
[51] Jones W.P., Marquis A.J. & Vogiatzaki K.; 2014, "Large-Eddy Simulation of Spray Combustion in a Gas Turbine Combustor", Comb. Flame, **161**, p 222.
[52] Andreini A., Bertini D., Mazzei L. & Puggelli S.; 2016, "Assessment of a Numerical Procedure for Scale Resolved Simulations of Turbulent Spray Flames". XXXIX Meeting of the Italian Section of the Combustion Institute.
[53] Puggelli S., Paccati S., Bertini D., Mazzei L., Giusti A. & Andreini A.; 2018, "Multi-coupled Numerical Simulations of the DLR Generic Single Sector Combustor", Comb. Sci. Tech., **190**, p 1409.